scientific reports

Check for updates

OPEN

Ir impurities in α- and β-Ga_2O_3 and their detrimental effect on p-type conductivity

Aleksandrs Zachinskis[1], Jurij Grechenkov[1], Edgars Butanovs[1], Aleksandrs Platonenko[1], Sergei Piskunov[1], Anatoli I. Popov[1], Juris Purans[1]✉ & Dmitry Bocharov[1,2]✉

Recently gallium oxide (Ga_2O_3) has become one of the most actively studied materials due to its competitive electronic properties such as wide bandgap, high breakdown field, simple control of carrier concentration, and high thermal stability. These properties make gallium oxide a promising candidate for potential applications in high-power electronic devices. β-Ga_2O_3 crystals are commonly grown by the Czochralski method in an iridium (Ir) crucible. For this reason, Ir is often present in Ga_2O_3 crystals as an unintentional dopant. In this work the impact of Ir incorporation defects on potential p-type conductivity in β-Ga_2O_3 is studied by means of density functional theory. The metastable α -Ga_2O_3 phase was investigated as the model object to understand the processes caused by iridium doping in gallium oxide-based systems. Obtained results allow us to understand better the influence of Ir on Ga_2O_3 electronic structure, as well as provide interpretation for optical transitions reported in recent experiments.

Gallium oxide in its beta-phase (β-Ga_2O_3) is a wide bandgap (4.7–4.9 eV[1,2]) semiconductor that has recently drawn significant attention becoming one of the most actively studied materials. Its promising properties such as a wide bandgap, high breakdown field (8 MV/cm), and high thermal and chemical stability make β-Ga_2O_3 being a strong candidate for applications in high-power electronics[3,4], such as Schottky diodes[5,6] and field-effect transistors[7], as well as in Boltzmann thermometers[8], solar-blind ultraviolet (UV) photodetectors[4], scintillators[9], and others[10]. Monoclinic β-Ga_2O_3 is thermodynamically the most stable crystalline phase[11]. A metastable hexagonal α-Ga_2O_3 is structurally similar to the corundum and has a slightly wider band gap of 5.1–5.3 eV[12,13]. This phase can be obtained using various thin film deposition processes (*e.g.* radio frequency (RF) sputtering, halide vapor phase epitaxy (HVPE), molecular beam epitaxy (MBE), atomic layer deposition (ALD), mist chemical vapor deposition (mist-CVD))[14], and could overcome β-Ga_2O_3 in device performance[15].

Heterojunctions are necessary for many device applications, thus the control of n- and p-type conductivity is important. N-type doping is easily achievable through addition of Si, Sn, C and Ge impurities[16–18]. Oxygen vacancies, which are native defects, can also act as electron donors[19]. Nb doping has been suggested to achieve similar effect elsewhere[20]. While n-type Ga_2O_3 has been successfully synthesized, p-type doping remains yet a challenge[21]. Most promising candidates for p-type doping are Mg and N, although induced defects levels are relatively deep[17]. Ismam et al.[22] discuss the employment of H-interstitials to control both p- and n-nype conductivity, nevertheless the hole mobility is rather low. Theoretical studies propose N–P, Al–N, and In–N co-doping to obtain a conductivity of p-type[23,24]. Nonetheless, challenges remain plenty: oxygen vacancies tend to counteract the proposed acceptors, even though this may be solved by annealing in O-rich atmosphere, Mg defects and gallium vacancies that also act as acceptors are passivated by hydrogen[19,25], and thus holes become self-trapped near an oxygen atom[26].

β-Ga_2O_3 crystals are grown by Czochralski (CZ) method using iridium (Ir) crucible[27,28]. As a result, iridium is present in β-Ga_2O_3 as an unintentional dopant[27] and it is speculated that Ir dopant may affect the p-type conductivity[25]. In n-type β-Ga_2O_3 Ir is in Ir^{3+} charged state[17]. Ir^{4+} charged state is also possible at low enough Fermi level, which can be achieved by introducing Mg impurities[17,29]. According to calculations reported by Ritter et al. [25], Ir incorporates in octahedral Ga_{II} site. In the octahedral crystal field 5 *d* orbitals of Ir split into 3 t_{2g} low energy orbitals and 2 e_g orbitals with higher energy. Ir^{3+} ($5d^6$) has no electron paramagnetic resonance (EPR) signal because six *d* electrons occupy 3 t_{2g} orbitals ($\uparrow\downarrow\ \uparrow\downarrow\ \uparrow\downarrow$)[30]. Ir^{4+} ($5d^5$), on the other hand, has a spin state S=1/2 ($\uparrow\downarrow\ \uparrow\downarrow\ \uparrow$)[30].

[1]Institute of Solid State Physics, University of Latvia, 8 Kengaraga str., Riga LV-1063, Latvia. [2]Transport and Telecommunication Institute, 1 Lomonosova str., Riga LV-1019, Latvia. ✉email: juris.purans@cfi.lu.lv; dmitrijs.bocarovs@cfi.lu.lv

In Mg-doped samples IR absorption peak at around 5150 cm^{-1} was reported in several experiments[25,30–32]. Origin of the peak is attributed to Ir^{4+} impurity, specifically, to a *d*-*d* transition within t_{2g} orbitals. Additionally, Seyidov et al.[32] observed that the intensity of the 5150 cm^{-1} peak reached its maximum at optical excitation of 2.9 eV in ERS (Electronic Raman Scattering) experiment. The maximum of 2.9 eV was hypothetically assigned to transition from t_{2g} orbitals to e_g orbitals located in the conduction band.

In this study we investigated electronic properties of Ir doped β-Ga_2O_3 by means of Density Functional Theory (DFT) calculations implemented via CRYSTAL17 code[33,34], assessed the impact of iridium impurities on the possibility of p-type doping in this material as well as evaluated the undesirable effects associated with the presence of iridium impurities. The calculated formation energies, charge-state transition levels, and electronic band structure are compared with available experimental results. Additionally, we investigated the role of Ir impurities in α-Ga_2O_3 phase. In these calculations α-Ga_2O_3 was used as a model object for which the effect of iridium doping was evaluated, as well as the similarities and differences with the stable β-Ga_2O_3, in which iridium impurities occur during actual material synthesis, were analyzed in order to predict the processes that may occur, for example, in samples with a mixed phase content.

Results

Calculated equilibrium lattice constants of pure α-Ga_2O_3 and β-Ga_2O_3 showed excellent agreement with experimental data (see Table 1). The calculated indirect bandgap of 4.73 eV for β-Ga_2O_3 and 5.29 eV for α-Ga_2O_3 are also in agreement with those experimentally measured (see Table 1). Direct bandgap is about 0.05 eV wider and is equal to 4.78 eV for β-Ga_2O_3 at k-point Γ, while for α-Ga_2O_3 direct bandgap is 5.52 eV, which is 0.23 eV wider than indirect, also at Γ.

The calculated formation energies of iridium defects are shown in Fig. 1. Most favorable substitution site is octahedral Ga_{II} in β-Ga_2O_3, consistent with reported by Ritter et al.[25]. Assuming bandgap of 4.73 eV, calculated thermodynamic charge state transition level $\varepsilon(+/0)$ of Ir in Ga_{II} site in β-Ga_2O_3 is located 2.6 eV below the conduction band minimum (CBM). Value of 2.6 eV below CBM is in good agreement with that experimentally measured 2.2-2.3 eV below CBM[31].

Phase	Parameter	This work	Exp.
β	a, Å	12.261	12.214[35]
	b, Å	3.0436	3.0371[35]
	c, Å	5.8164	5.7981[35]
	β	103.83^o	103.83^o[35]
	bandgap, eV	4.73	4.7[1]
α	a, Å	4.9953	4.9825[36]
	c, Å	13.408	13.433[36]
	bandgap, eV	5.29	5.27-5.3[12,37,38]

Table 1. Lattice constants and bandgap energy of pure α-Ga_2O_3 and β-Ga_2O_3 phases calculated with hybrid functional HSE06 and double-zeta basis set. Experimental data is given for reference.

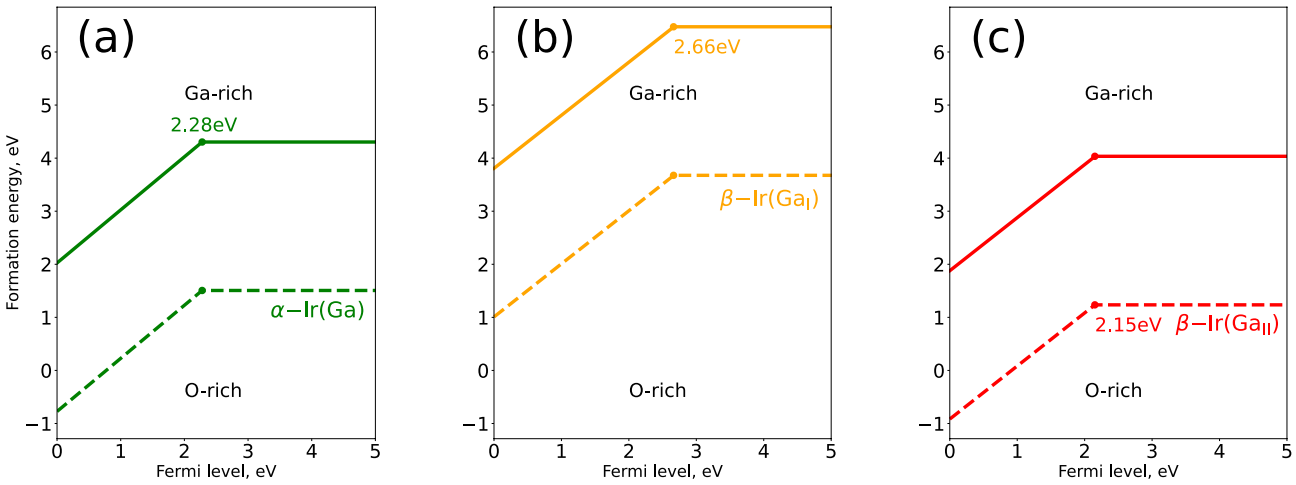

Figure 1. Formation energy of Ir substitution defects in both α-Ga_2O_3 (**a**) and β-Ga_2O_3 ((**b**) for Ir atom in Ga_I and (**c**) for Ir atom in Ga_{II} two nonequivalent position, correspondingly) and as calculated according to Eq. (2). Solid and dashed lines correspond to Ga-rich and O-rich conditions, respectively.

Iridium in β-Ga_2O_3 was observed in Ir^{3+} ($5d^6$) and Ir^{4+} ($5d^5$) states[30]. Under the influence of a strong crystal field, d-orbitals split. According to our calculations, the ground state of Ir^{3+} in both nonequivalent sites is non-magnetic (S=0) ($\uparrow\downarrow\uparrow\downarrow\uparrow\downarrow$). On the other hand, Ir^{4+} in octahedral $Ir_{Ga_{II}}$ and tetrahedral Ir_{Ga_I} sites converge to spin state S = 1/2 ($\uparrow\downarrow\uparrow\downarrow\uparrow$). This result is in agreement with EPR experiment[30]. We investigated spin states further, and found that for $Ir^{3+}_{Ga_I}$ spin states S=2/2 and S=4/2 are 0.3 eV and 1.1 eV more favorable than S=0, respectively. The spin states of both $Ir^{3+}_{Ga_{II}}$ and Ir^{3+}_{Ga} (in α-Ga_2O_3) also converged to S=4/2. They are 3.8 eV more favorable with respect to S=0. $Ir^{4+}_{Ga_I}$ also converged to S=3/2, which is 0.9 eV more favorable than S=1/2. High-spin configuration S=5/2 is not predicted for Ir^{4+} substitution dopant.

Kohn-Sham levels of Ir for both α-Ga_2O_3 and β-Ga_2O_3 from band structure calculations are illustrated in Fig. 2. Energy levels located in the conduction band were also added. IR peak at 5150 cm^{-1} (0.64 eV) was observed in several experiments and attributed to a transition within t_2g orbitals in iridium atom substituting octahedral Ga_{II} in β-Ga_2O_3. The intensity of 5150 cm^{-1} peak was at a maximum when the sample was irradiated with 2.9 eV light[32]. The energy of 2.9 eV was hypothetically attributed to electronic transition in $Ir^{4+}(Ga_{II})$ between t_{2g} and e_g orbitals in β-Ga_2O_3, assuming e_g orbitals are located in conduction band[32].

From the calculated band structure we see a possible electronic transition in $Ir^{4+}(Ga_{II})$ (last column) at the energy of 3.0 eV in β-Ga_2O_3 that most likely correspond to 2.9 eV transition reported by Seyidov et.al.[32]. Furthermore, we see two possible transitions with the energy of around 0.5 eV (≈4000 cm^{-1}) that most likely correspond to 5150 cm^{-1} peak. One can further conclude that the transitions of the defect from a Ir^{3+} to a Ir^{4+} state at a certain Fermi level leads to Ir acting as a hole trap.

In other words iridium defects inhibit the p-type conductivity in the material after the hole concentration reaches a certain level. This concentration can be estimated by the use of the mass action law[39]:

$$p = N_v e^{\left(-\frac{E_F - E_V}{k_B T}\right)} \tag{1}$$

where p is hole concentration, E_F—Fermi level E_V—valence band energy, and N_v—hole concentration at valence band edge.

From our computations $E_V - E_{F,critical} \approx 2.7\ eV$ and the number of states in a ≈ 25 meV close to the valence band edge is $N_V \approx 0.11$ per unit cell. Assuming room temperature ($T = 300$ K), one can obtain a noticeably low hole concentration of $p \approx 3 \times 10^{-15}$ cm^{-3} that should be approximately equal to the dopant concentration, for which the effect takes place.

Additionally, from Fig. 2 we can conclude following statements about Ir dopants β-Ga_2O_3:

1. The indirect bang gap of 4.78 eV in β-Ga_2O_3 practically does not change when iridium impurities are introduced.

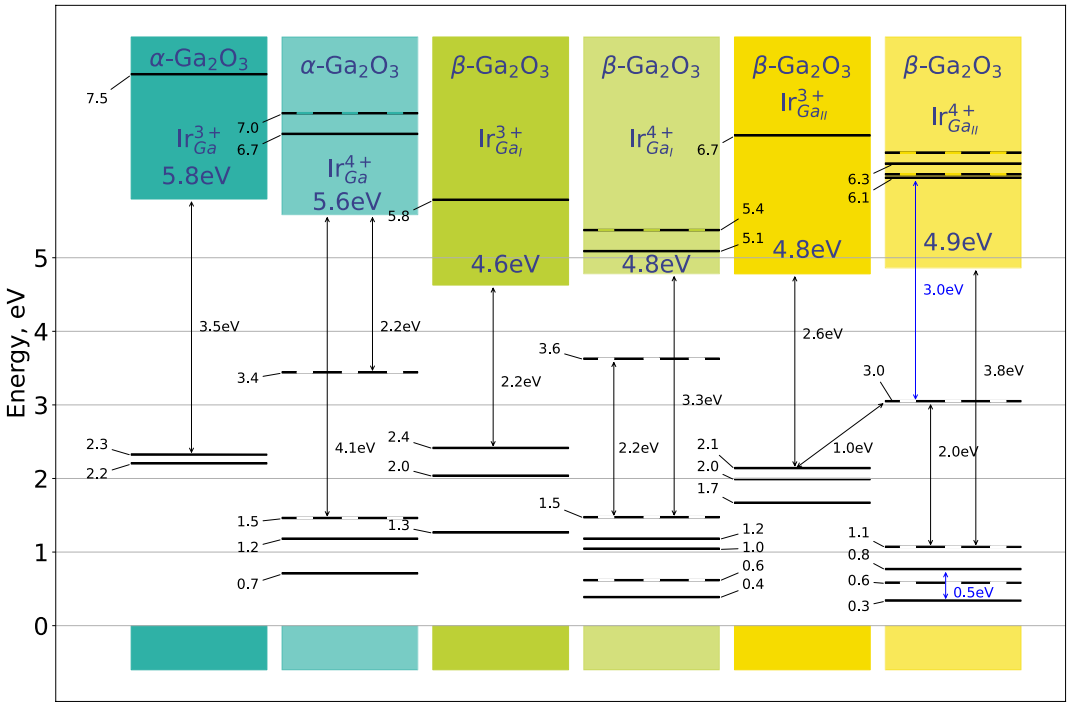

Figure 2. Schematic illustration of band structure of α-Ga_2O_3 and β-Ga_2O_3 with Ir impurities. Solid and dashed lines distinguish between alpha and beta electrons. All energy levels were evaluated at k-point Γ. Energy levels of Ir in the conduction band were also included. All valence band maxima were aligned and set to zero energy.

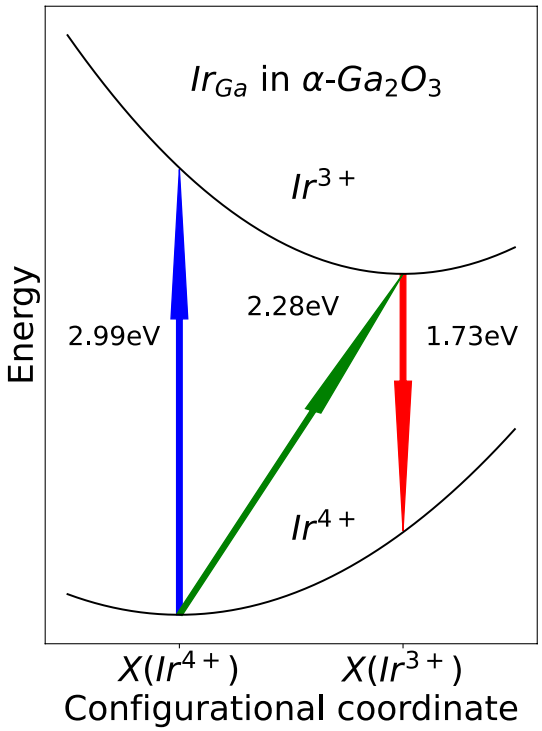

Figure 3. Configurational diagram of optical transition levels of $Ir_{Ga_{II}}$ in β-Ga_2O_3 and Ir_{Ga} in α-Ga_2O_3, exchanging an electron with valence band. $X(Ir^{4+})$ and $X(Ir^{3+})$ corresponds to the geometry of the ground state of Ir^{4+} and Ir^{3+}, respectively.

2. The position of the levels in the band gap depends on the Ga-ion position in which it is located. Moreover, this is true for both charge states of iridium, namely, Ir^{3+} and Ir^{4+}.
3. In the case of Ir^{3+}, the position of its ground state with respect to the bottom of the conduction band is 2.2 eV and 2.6 eV for Ga_I site and Ga_{II} site, respectively. These energies formally correspond to the ionization energy $Ir^{3+} \rightarrow Ir^{4+}$, this difference should be easily distinguishable in the experiment. Note that the threshold for exciting an electron from the Ir^{3+} level to the conduction band minimum was found to be between 2.2 and 2.3 eV[31], which corresponds to the position of iridium in Ga_I.
4. Strange as it may seem, but only for Ga_I position our calculations show the presence of an excited quasi-local state Ir^{3+}, which is higher than the bottom of CB by about 1 eV. Furthermore, we can assume the presence of the optical absorption band of Ir^{3+} at 3.2 eV.
5. The presence of an unoccupied level of $Ir^{3+}(Ga_I)$ in the conduction band hints to a possibility of it being a center of an electron capture with the formation of transient states of Ir^{2+}, according to the following reaction: $Ir^{3+} + e \rightarrow Ir^{2+}$. Note that a summary of Ir^{2+} ions in the different compound was done by Pidol[40] *et.al.*.

Following the work of Ritter et al.[25] we calculated also optical transition levels of $Ir_{Ga_{II}}$ in β-Ga_2O_3 and Ir_{Ga} in α-Ga_2O_3. The difference between thermodynamic and optical charge state transition levels is that no relaxation of geometry is performed. Results are illustrated in the Fig. 3. Absorption and emission energy (blue and red arrow, respectively) differs by about 0.6 eV from thermodynamics transition for both α and β phases.

Methods

DFT calculations. DFT calculations were performed using linear combination of atomic orbitals (LCAO) method and HSE06 hybrid exchange-correlation functional[41]. In the DFT method, the energy of a system is expressed as a functional of the spatial electron density. Hybrid functionals, like HSE06, are designed to overcome some of the limitations of traditional DFT functionals by incorporating a certain amount of exact exchange energy. The screening parameter in HSE06 determines the range separation between short- and long-range interactions in the functional. This screened Coulomb potential weakens the long-range contribution of the exact exchange mitigating the self-interaction error frequently observed in standard DFT functionals. The HSE06 functional incorporates a 25 % short-range Hartree-Fock exchange without any long-range Hartree-Fock exchange. In the most recent version of the functional, the screening parameter is chosen empirically and assigned a value of 0.11 $Bohr^{-1}$.[42] Gaussian type double-zeta basis sets developed by Vilela Oliveira et al.[43] were used for O and Ga atoms. A double-zeta basis set in LCAO method employs two basis functions for each atomic orbital instead of just one, as in a single-zeta basis set. This means that for each AO in the atom, there are two functions with different radial extents (contraction coefficients) and adjustable weights. The purpose of using two functions is to provide a more flexible representation of the electron distribution around the nucleus,

thereby improving the description of molecular orbitals and the overall accuracy of the calculations. For the Ir atom an effective core triple-zeta split-valence plus polarization pseudopotential basis set was taken in the form as it was suggested by Pint et al.[44] and Chesnokov et al.[45].

The supercell approach was adopted to model isolated Ir defect. A 120 atom 1×3×2 supercell (relative to crystallographic cell) was used for β-Ga_2O_3. The same 120 atom size 2×2×1 supercell was utilized for α-Ga_2O_3 calculations. 4×4×4 Pack-Monkhorst net was used, resulting in 36 k-points in the first Brillouin zone. The threshold for the energy convergence in self-consistent field (SCF) procedure was set to be 10^{-7} Hartree. Complete relaxation of atomic coordinates has been performed. Other computational parameters were left as default (see CRYSTAL17 manual[33]).

Formation energies of Ir defects were calculated using the relation:

$$E^f = E[X^q] - E[I] - \sum_i n_i\mu_i + qE_F + E_{\text{corr}} \tag{2}$$

$E[X^q]$ is the total energy of a defective system with a charge q, $E[I]$ is the total energy of an ideal system, n_i is a number of added atoms with chemical potential μ_i (if an atom was removed, then n_i is negative), E_F is the Fermi level relative to valence band maximum (VBM) and E_{corr} is the correction energy due to electrostatic interactions of charged defects. For the charged Ir^{4+} ions, correction energy E_{corr} for first order electrostatic interactions is calculated following the Makov-Payne correction scheme[46]. We follow the methodology of computing correction energy in the CRYSTAL code as is described by Bailey et al. [47]. For more details, see the next subsection.

Since chemical potentials may vary depending on experimental conditions we considered two limiting scenarios, namely, O-rich and Ga-rich (O-poor) conditions. In the O-rich condition, the system is assumed to have a high concentration of oxygen compared to gallium. The chemical potential of oxygen is then calculated based on the total energy of an oxygen molecule, *i.e.* half of the total energy of an O_2 was taken as μ for O. The μ_O is considered as the reference point, and the chemical potential of gallium is then calculated based on the total energy of Ga_2O_3. On the other hand, in the Ga-rich condition, the system is assumed to have a high concentration of gallium compared to oxygen. The chemical potential of gallium for Ga-rich condition was taken from the total energy calculation of metallic gallium in its alpha phase. The chemical potential of Ir was determined from total energy calculations of IrO_2 and metallic Ir in the O-rich and Ga-rich limits, respectively.

Estimation of correction energy. One of the challenges of the present work was to properly estimate the correction energy of charged defects E_{corr}, which is used to calculate the formation energy of the charged point defects.

The origin of the term E_{corr} in Eq. (2) comes from using periodic boundary conditions. Clearly, the unit cell of the crystal cannot be charged, because in that case, the total energy would diverge. Because of that, any additional charge in the cell is compensated with a homogeneous background charge that ensures the neutrality of the cell. The correction energy accounts for the Coulomb interactions of the mirror images of the defects, as well as defect-background and background-background interactions.

To estimate the correction energy using CRYSTAL17 code[33] we followed the methodology proposed in Ref.[47]. E_{corr} consists of two parts. The first part, which is commonly is denoted as ΔV, is the difference between the reference points of electrostatic potentials of neutral and charged systems. In non-periodic systems the reference point (or 0 value) is usually taken at the infinity distance, which is universal for all non-periodic systems. In periodic systems, however, there is no such point. Because of this we need to calculate a constant offset ΔV of the electrostatic potentials to compare the energies of two systems, namely, neutral and charged.

Following Ref.[47], ΔV was calculated as a difference between the total energies of two systems: neutral defect-free system of infinitely large supercell and the same system, but without one electron. Of course, it is impossible to use the infinite supercell practically, instead, one should look at the tendency of ΔV with supercell size tending to infinity.

As it can be seen from Fig. 4, we calculated the needed difference at 10, 20, 120, 240 and 360 atoms in the supercell for β-Ga_2O_3. The results for cells with 240 and 360 atoms differ by less than 0.01 eV. We assumed the value of ΔV to be 8.48 eV with a possible error of 0.01 eV. Similarly, we did the same calculations for α-Ga_2O_3 and got the value of ΔV of 9.70 eV. The total energy of charged system should be corrected by this number times the charge of the unit cell $q\Delta V$.

The second part of the correction energy, which we denote as ΔE, includes Coulomb interactions between charged point defect and it's mirror images. Theoretically, it can be calculated using the formula[46]:

$$\Delta E = \frac{q^2\alpha_M}{2\varepsilon L} + O(L^{-3}) \tag{3}$$

where q is the charge of the defect, α_M is the Madelung constant for the specific lattice, L is linear size of the cell and ε is the dielectric constant. The value of $\frac{\alpha_M}{2L}$ can be directly computed with CRYSTAL code. In order to obtain it, we ran a calculation with the only atom in the supercell being the hydrogen atom located at a defect site. $\frac{\alpha_M}{2L}$ is the nucleus-nucleus interaction of the resulting system, which can be directly gathered from the calculation output. Dielectric constant ε can be taken from literature or calculated directly with CRYSTAL17. In our work we took ε from the literature (β-Ga_2O_3: $\varepsilon = 3.56$[48], α-Ga_2O_3: $\varepsilon = 3.75$[49]). With our supercell size (120 atoms, volume is around 1000 $Å^3$) ΔE turned out to be 0.5 eV.

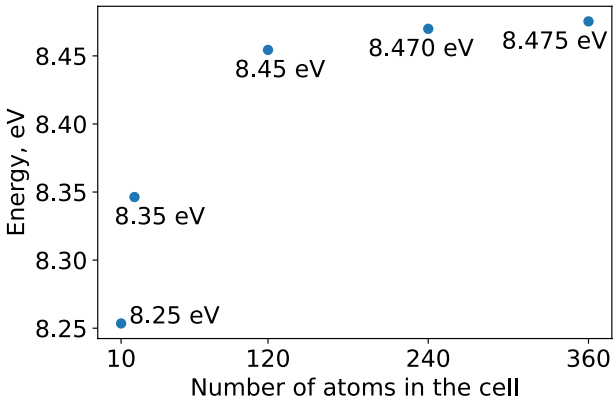

Figure 4. Energy difference between the β-Ga_2O_3 without one electron and ideal β-Ga_2O_3 at different supercell sizes with 10, 20, 120, 240 and 360 atoms.

Conclusions

We calculated band structure and formation energies of iridium defects in β-Ga_2O_3 and α-Ga_2O_3. In β-Ga_2O_3 octahedral site is highly more favorable for substitution than tetrahedral. From band structure calculations we predict electronic transitions with the energies of 0.5 and 3.0 eV, that most likely correspond to experimentally observed absorption energies at 5150 cm^{-1} (0.64 eV) and 2.9 eV in β-Ga_2O_3. We justify that the origin of these energies indeed is the transitions between *d* orbitals in Ir^{4+} substituting octahedrally coordinated gallium (Ga_{II}).

Defect formation energy diagram points to the fact that Iridium impurities in Czochralski grown β-Ga_2O_3 mono-crystals inhibit p-type conductivity. This prediction is in agreement with previously published studies[25] and should be taken into account considering Ga_2O_3 as a p-type material (Supplementary File 1).

Data availibility

The datasets used and analyzed during the current study are included in this published article in supplementary information as Supplementary File. "S1. Archive with input/output data of CRYSTAL code calculations".

Received: 28 February 2023; Accepted: 12 May 2023
Published online: 26 May 2023

References

1. Tippins, H. H. Optical absorption and photoconductivity in the band edge of β-Ga_2O_3. *Phys. Rev.* **140**, A316–A319. https://doi.org/10.1103/PhysRev.140.A316 (1965).
2. Janowitz, C. *et al.* Experimental electronic structure of In_2O_3 and Ga_2O_3. *New J. Phys.* **13**, 085014. https://doi.org/10.1088/1367-2630/13/8/085014 (2011).
3. Pearton, S. J. *et al.* A review of Ga_2O_3 materials, processing, and devices. *Appl. Phys. Rev.* **5**, 011301. https://doi.org/10.1063/1.5006941 (2018).
4. Zhang, J., Shi, J., Qi, D.-C., Chen, L. & Zhang, K. H. L. Recent progress on the electronic structure, defect, and doping properties of Ga_2O_3. *APL Mater.* **8**, 020906. https://doi.org/10.1063/1.5142999 (2020).
5. Khartsev, S., Nordell, N., Hammar, M., Purans, J. & Hallén, A. High-quality si-doped β-Ga_2O_3 films on sapphire fabricated by pulsed laser deposition. *Phys. Status Solidi (b)* **258**, 2000362 (2021).
6. Khartsev, S. *et al.* Reverse-bias electroluminescence in er-doped β-Ga_2O_3 schottky barrier diodes manufactured by pulsed laser deposition. *Phys. Status Solidi a* **219**, 2100610. https://doi.org/10.1002/pssa.202100610 (2022).
7. Ro, H.-S., Kang, S. H. & Jung, S. The effect of gate work function and electrode gap on wide band-gap sn-doped α-Ga_2O_3 metal; Semiconductor field-effect transistors. *Materials*https://doi.org/10.3390/ma15030913 *(2022).*
8. Back, M. *et al.* Boltzmann thermometry in cr^{3+}-doped Ga_2O_3 polymorphs: The structure matters! Adv. *Opt. Mater.* **9**, 2100033. https://doi.org/10.1002/adom.202100033 (2021).
9. Mykhaylyk, V. B., Kraus, H., Kapustianyk, V. & Rudko, M. Low temperature scintillation properties of Ga_2O_3. *Appl. Phys. Lett.* **115**, 081103. https://doi.org/10.1063/1.5119130 (2019).
10. Green, A. J. *et al.*β-gallium oxide power electronics. *APL Mater.* **10**, 029201. https://doi.org/10.1063/5.0060327 (2022).
11. Bosi, M., Mazzolini, P., Seravalli, L. & Fornari, R. Ga_2O_3 polymorphs: Tailoring the epitaxial growth conditions. *J. Mater. Chem. C* **8**, 10975–10992. https://doi.org/10.1039/D0TC02743J (2020).
12. Shinohara, D. & Fujita, S. Heteroepitaxy of corundum-structured α-Ga_2O_3 thin films on α-Al_2O_3 substrates by ultrasonic mist chemical vapor deposition. *Jpn. J. Appl. Phys.* **47**, 7311–7313. https://doi.org/10.1143/jjap.47.7311 (2008).
13. Chen, X. *et al.* Solar-blind photodetector with high avalanche gains and bias-tunable detecting functionality based on metastable phase α-Ga_2O_3/zno isotype heterostructures. *ACS Appl. Mater.* **9**, 36997–37005. https://doi.org/10.1021/acsami.7b09812 (2017) (**PMID: 28975779**).
14. Yang, D., Kim, B., Eom, T. H., Park, Y. & Jang, H. W. Epitaxial growth of alpha gallium oxide thin films on sapphire substrates for electronic and optoelectronic devices: Progress and perspective. *Electron. Mater. Lett.* **18**, 113–128. https://doi.org/10.1007/s13391-021-00333-5 (2022).
15. Ahmadi, E. & Oshima, Y. Materials issues and devices of α- and β-Ga_2O_3. *J. Appl. Phys.* **126**, 160901. https://doi.org/10.1063/1.5123213 (2019).
16. Anhar Uddin Bhuiyan, A. F. M. *et al.* MOCVD epitaxy of β-$(Al_xGa_{1-x})_2O_3$ thin films on (010) Ga_2O_3 substrates and N-type doping. *Appl. Phys. Lett.* **115**, 120602. https://doi.org/10.1063/1.5123495 (2019).
17. McCluskey, M. D. Point defects in Ga_2O_3. *J. Appl. Phys.* **127**, 101101. https://doi.org/10.1063/1.5142195 (2020).

18. Rafique, S. *et al.* Heteroepitaxy of N-type β-Ga_2O_3 thin films on sapphire substrate by low pressure chemical vapor deposition. *Appl. Phys. Lett.* **109**, 132103 (2016).
19. Tadjer, M. J. *et al.* Theory and characterization of doping and defects in β-Ga_2O_3. *ECS J. Solid. State. Sci. Technol.* **8**, Q3187. https://doi.org/10.1149/2.0341907jss (2019).
20. Zhou, W., Xia, C., Sai, Q. & Zhang, H. Controlling n-type conductivity of β-Ga_2O_3 by Nb doping. *Appl. Phys. Lett.* **111**, 242103. https://doi.org/10.1063/1.4994263 (2017).
21. Kyrtsos, A., Matsubara, M. & Bellotti, E. On the feasibility of p-type Ga_2O_3. *Appl. Phys. Lett.* **112**, 032108. https://doi.org/10.1063/1.5009423 (2018).
22. Islam, M. M. *et al.* Chemical manipulation of hydrogen induced high p-type and n-type conductivity in Ga_2O_3. *Sci. Rep.* **10**, 6134. https://doi.org/10.1038/s41598-020-62948-2 (2020).
23. Li, L., Liao, F. & Hu, X. The possibility of N-P codoping to realize P type β-Ga_2O_3. *Superlattices Microstruct.* **141**, 106502. https://doi.org/10.1016/j.spmi.2020.106502 (2020).
24. Ma, J. *et al.* Achieving high conductivity p-type Ga_2O_3 through Al-N and In-N co-doping. *Chem. Phys. Lett.* **746**, 137308. https://doi.org/10.1016/j.cplett.2020.137308 (2020).
25. Ritter, J. R. *et al.* Compensation and hydrogen passivation of magnesium acceptors in β-Ga_2O_3. *Appl. Phys. Lett.* **113**, 052101. https://doi.org/10.1063/1.5044627 (2018).
26. Varley, J. B., Janotti, A., Franchini, C. & Van de Walle, C. G. Role of self-trapping in luminescence and *p*-type conductivity of wide-band-gap oxides. *Phys. Rev. B* **85**, 081109. https://doi.org/10.1103/PhysRevB.85.081109 (2012).
27. Galazka, Z. *et al.* Scaling-up of bulk β-Ga_2O_3 single crystals by the czochralski method. *ECS J. Solid State Sci. Technol.* **6**, Q3007–Q3011. https://doi.org/10.1149/2.0021702jss (2017).
28. Drozdowski, W. *et al.* Semiconductor scintillator development: Pure and doped β-Ga_2O_3. *Opt. Mater.* **105**, 109856. https://doi.org/10.1016/j.optmat.2020.109856 (2020).
29. Luchechko, A., Vasyltsiv, V., Kostyk, L., Tsvetkova, O. & Popov, A. Shallow and deep trap levels in x-ray irradiated β-Ga_2O_3: Mg. *Nucl. Instrum. Methods Phys. Res. B.* **441**, 12–17. https://doi.org/10.1016/j.nimb.2018.12.045 (2019).
30. Lenyk, C. A. *et al.* Ir $^{4+}$ ions in β-Ga_2O_3 crystals: An unintentional deep donor. *J. Appl. Phys.* **125**, 045703. https://doi.org/10.1063/1.5081825 (2019).
31. Ritter, J. R., Lynn, K. G. & McCluskey, M. D. Iridium-related complexes in czochralski-grown β-Ga_2O_3. *J. Appl. Phys.* **126**, 225705. https://doi.org/10.1063/1.5129781 (2019).
32. Seyidov, P., Ramsteiner, M., Galazka, Z. & Irmscher, K. Resonant electronic raman scattering from ir^{4+} ions in β-Ga_2O_3. *Appl. Phys. Lett.* **131**, 035707. https://doi.org/10.1063/5.0080248 (2022).
33. Dovesi, R. *et al. CRYSTAL17 User's Manual* (University of Torino, 2017).
34. Dovesi, R. *et al.* Quantum-mechanical condensed matter simulations with crystal. *Wiley Interdiscip. Rev. Comput. Mol. Sci.*https://doi.org/10.1002/wcms.1360 *(2018).*
35. Åhman, J., Svensson, G. & Albertsson, J. A reinvestigation of β-gallium oxide. *Acta. Crystallogr. C Cryst. Struct. Commun.* **52**, 1336–1338. https://doi.org/10.1107/S0108270195016404 (1996).
36. Marezio, M. & Remeika, J. P. Bond lengths in the α-Ga_2O_3 structure and the high-pressure phase of $ga_{2-x}fe_xo_3$. *Chem. Phys.* **46**, 1862–1865. https://doi.org/10.1063/1.1840945 (1967).
37. Akaiwa, K. & Fujita, S. Electrical conductive corundum-structured α-Ga_2O_3 thin films on sapphire with tin-doping grown by spray-assisted mist chemical vapor deposition. *Jpn. J. Appl. Phys.* **51**, 070203. https://doi.org/10.1143/jjap.51.070203 (2012).
38. Hao, J. *et al.* Phase tailoring and wafer-scale uniform hetero-epitaxy of metastable-phased corundum α-Ga_2O_3 on sapphire. *J. Appl. Phys.* **513**, 145871. https://doi.org/10.1016/j.apsusc.2020.145871 (2020).
39. Sze, S. & Ng, K. K. *Physics of Semiconductor Devices* (Wiley, 2006).
40. Pidol, L. *et al.* Scintillation properties of $Lu_2Si_2O_7:Ce^{3+}_3$, a fast and efficient scintillator crystal. *J. Phys. Condens. Matter* **15**, 2091. https://doi.org/10.1088/0953-8984/15/12/326 (2003).
41. Heyd, J., Scuseria, G. E. & Ernzerhof, M. Hybrid functionals based on a screened coulomb potential. *J. Chem. Phys.* **118**, 8207–8215. https://doi.org/10.1063/1.1564060 (2003).
42. Janesko, B. G., Henderson, T. M. & Scuseria, G. E. Screened hybrid density functionals for solid-state chemistry and physics. *Phys. Chem. Chem. Phys.* **11**, 443–454. https://doi.org/10.1039/B812838C (2009).
43. Vilela Oliveira, D., Laun, J., Peintinger, M. F. & Bredow, T. BSSE-correction scheme for consistent gaussian basis sets of double-and triple-zeta valence with polarization quality for solid-state calculations. *J. Comput. Chem.* **40**, 2364–2376. https://doi.org/10.1002/jcc.26013 (2019).
44. Ping, Y., Galli, G. & Goddard, W. A. Electronic structure of IrO_2: The role of the metal d orbitals. *J. Phys. Chem. C* **119**, 11570–11577. https://doi.org/10.1021/acs.jpcc.5b00861 (2015).
45. Chesnokov, A. *et al.* The local atomic structure and thermoelectric properties of ir-doped ZnO: Hybrid DFT calculations and XAS experiments. *J. Mater. Chem. C* **9**, 4948–4960. https://doi.org/10.1039/D1TC00223F (2021).
46. Makov, G. & Payne, M. C. Periodic boundary conditions in ab initio calculations. *Phys. Rev. B* **51**, 4014–4022. https://doi.org/10.1103/PhysRevB.51.4014 (1995).
47. Bailey, C. L., Liborio, L., Mallia, G., Tomić, S. & Harrison, N. M. Calculating charged defects using CRYSTAL. *J. Phys. Conf. Ser.* **242**, 012004. https://doi.org/10.1088/1742-6596/242/1/012004 (2010).
48. Schubert, M. *et al.* Anisotropy, phonon modes, and free charge carrier parameters in monoclinic β-gallium oxide single crystals. *Phys. Rev. B* **93**, 125209. https://doi.org/10.1103/PhysRevB.93.125209 (2016).
49. Feneberg, M. *et al.* Ordinary dielectric function of corundumlike α-Ga_2O_3 from 40 mev to 20 ev. *Phys. Rev. Mater.* **2**, 044601. https://doi.org/10.1103/PhysRevMaterials.2.044601 (2018).

Acknowledgements

This research is funded by the Latvian Council of Science project "Epitaxial Ga_2O_3 thin films as ultrawide band-gap topological transparent electrodes for ultraviolet optoelectronics" No. lzp-2020/1-0345. Institute of Solid State Physics, University of Latvia as the Center of Excellence has received funding from the European Union's Horizon 2020 Framework Programme H2020-WIDESPREAD-01-2016-2017-TeamingPhase2 under grant agreement No. 739508, project $CAMART^2$.

Author contributions

Conceptualization, A.Z., S.P., J.P., and D.B.; methodology, A.Z., A.P., S.P., and D.B.; software, A.Z.; validation, A.Z., J.G., E.B., A.P., J.P., S.P., and D.B.; formal analysis, A.Z. and J.G.; investigation, A.Z.; resources, A.P.; data curation, A.Z.; writing—original draft preparation, A.Z., J.G., and D.B.; writing—review and editing, J.G., E.B., S.P., A.I.P., and D.B.; visualization, A.Z.; supervision, S.P., J.P. and D.B.; project administration J.P.; funding acquisition: J.P. All authors have read and agreed to the published version of the manuscript. The authors are greatly indebted to Prof. M.G. Brik for many stimulating discussions.

Competing interests
The authors declare no competing interests.

Additional information
Supplementary Information The online version contains supplementary material available at https://doi.org/10.1038/s41598-023-35112-9.

Correspondence and requests for materials should be addressed to J.P. or D.B.

Reprints and permissions information is available at www.nature.com/reprints.

Publisher's note Springer Nature remains neutral with regard to jurisdictional claims in published maps and institutional affiliations.